Polymers for Advanced Technologies

WILEY

polymers advanced technologies

RESEARCH ARTICLE OPEN ACCESS

Microalgae-Mediated Synthesis and Characterization of Metal Oxide Nanoparticles for Potential Enhancement of Tomato Plant Growth and Their Effects on Methylene Blue Dye Degradation

Anab Mujtaba[1] | Marfaa Naseem[1] | Rameesha Abid[1] | Muhammad Ishtiaq Ali[1] | Rabia Asghar[1] | Asif Jamal[1] | Xin Sun[2] | Yusuf Tutar[2] | Ahsan Habib[3,4,5] | Bakhtiyar Badalov[6]

[1]Department of Microbiology, Quaid-i-Azam University, Islamabad, Pakistan | [2]Division of Biochemistry, Department of Basic Medical Sciences, Faculty of Medicine, Recep Tayyip Erdogan University, Rize, Türkiye | [3]Department of Textile Engineering Management, Bangladesh University of Textiles, Dhaka, Bangladesh | [4]Department of Textile Engineering, Engineering Faculty, Cukurova University, Adana, Turkey | [5]Institut für Textiltechnik, RWTH Aachen University, Aachen, Germany | [6]Xi'an University of Architecture and Technology, Xi'an, China

Correspondence: Muhammad Ishtiaq Ali (ishimrl@qau.edu.pk) | Ahsan Habib (habibtexm@gmail.com)

Received: 23 February 2026 | **Revised:** 10 April 2026 | **Accepted:** 24 April 2026

Keywords: antimicrobial activity | biofertilizer | biosynthesized nanoparticles | microalgae | photocatalytic degradation

ABSTRACT

Agricultural productivity and environmental quality are increasingly threatened by the limitations and hazards associated with conventional chemical inputs. To address this, the present study explores the biosynthesis of metal oxide nanoparticles using microalgal extracts of *Tetradesmus nygardii* and evaluates their potential as biofertilizers, antifungal agents, and photocatalytic materials. Synthesized nanoparticles were structurally and optically characterized by UV–Visible spectroscopy, Fourier transform infrared spectroscopy (FTIR), and X-ray diffraction (XRD), which confirmed phase-pure crystalline formation at nanoscale dimensions. AgONPs exhibited ultra-small crystallites (1.23–2.70 nm), while CuONPs and NiONPs ranged from 11.2–13.9 nm and 11.8–18.9 nm, respectively. When applied to tomato (*Solanum lycopersicum*) plants, AgONPs produced a 166% increase in chlorophyll content (37.8 μmol m^{-2}) and a shoot fresh weight of 4.5 g, while reducing disease prevalence from 38.46% to 3.03%. A combined nanoparticle treatment further reduced disease incidence to 6.25% and extended shoot length to 55 cm, indicating synergistic growth-promoting effects. In antifungal assays against *Rhizopus* spp., complete inhibition was recorded at 200 μg/mL across all tested nanoparticles, with AgONPs and ZnONPs showing superior dose-dependent activity. For photocatalytic performance, AgONPs achieved a methylene blue degradation efficiency of 98.27% under sunlight at a rate of 30.84%/h. These results highlight microalgae-derived AgONPs as a multifunctional and scalable solution for enhancing crop health, controlling phytopathogens and degrading textile dye pollutants, offering a sustainable alternative to synthetic agrochemicals and chemical-based remediation approaches.

1 | Introduction

Modern agricultural practices heavily rely on synthetic fertilizers and agrochemicals to enhance crop yields. However, this extensive dependence has led to considerable environmental challenges, including soil degradation, biodiversity loss, and increased greenhouse gas emissions [1]. Overuse of chemical fertilizers contributes to soil acidification and disrupts natural ecosystems, while also contributing substantially to nitrous oxide emissions, a greenhouse gas with a global warming potential

Correction added on 20 May 2026, after first online publication: The copyright line was changed.

nearly 300 times that of carbon dioxide. Beyond environmental concerns, the excessive use of chemical fertilizers poses serious health risks. Nitrates leaching into groundwater contaminates drinking water sources, causing methemoglobinemia ("blue baby syndrome") and raising the risk of certain cancers in exposed populations. Moreover, continuous chemical inputs have weakened crop resilience, making plants like tomatoes more susceptible to fungal diseases Fusarium and Rhizopus infections. These environmental and health risks highlight the urgent need to reconsider current fertilizer practices and seek sustainable alternatives.

Globally, over 120 million tons of synthetic fertilizers are used annually, accounting for approximately 40% of agriculture-related greenhouse gas emissions. Despite this massive input, nutrient use efficiency remains low, with only 30%–50% of nitrogen, 45% of phosphorus, and 30%–40% of potassium being absorbed by crops, with the remainder lost to leaching and volatilization [2]. This inefficiency not only wastes resources but also exacerbates environmental pollution. In Pakistan, these challenges are more pronounced. Agriculture accounts for about 23% to the national GDP (Gross Domestic Product) and employs over 42% of the population. Fertilizer uses 133 kg per hectare, significantly exceeding the global average of 94 kg/ha, yet substantial yield gaps persist. Rising fertilizer costs, including urea prices reaching nearly PKR 4000 per 50 kg bag, further strain smallholder farmers.

To address these challenges, the focus has shifted towards biofertilizers as environmentally responsible alternatives. While compost and organic manure can improve soil texture, they often act slowly and lack adequate nutrient density. Similarly, microbial-based inoculants may face challenges in degraded or monoculture soils due to poor establishment and inconsistent effectiveness. This highlights the need for sustainable and scalable biological inputs that not only enhance crop yields but also strengthen plant defense mechanisms without causing environmental harm.

Microalgae offer a promising solution as sustainable biofertilizers. These photosynthetic microorganisms, with over 25,000 documented species, thrive in freshwater and marine environments. Notable genera such as *Chlorella*, *Spirulina*, and *Tetradesmus* are rich in biologically active compounds, including proteins, carbohydrates, lipids, vitamins, and pigments [3]. Their cultivation does not require fertile land and can utilize wastewater, making the process both cost-effective and eco-friendly. Microalgal biomass has demonstrated potential to increase chlorophyll content, improve nutrient uptake, and enhance natural plant resistance against pathogens [4]. Recent advances in green nanotechnology have highlighted the biosynthesis of metal nanoparticles using microalgal extracts as a sustainable approach. In this process, metal salts are reduced by bioactive compounds naturally present in microalgae, such as proteins, polysaccharides, and phenolics, thereby eliminating the need for hazardous chemical reducing agents and stabilizers. This sustainable synthesis method not only reduces ecological impacts but also yields nanoparticles with biocompatible surface coatings, enhanced stability and improved functional properties. Metal-based nanoparticles produced through this route, including silver (Ag), copper (Cu), nickel (Ni), and zinc (Zn), have demonstrated strong antimicrobial, antifungal, and photocatalytic activities in various studies [5–7]. Additionally, the microalgae-mediated synthesis of metal oxide nanoparticles offers a cost-effective alternative to chemical fertilizers from an economic standpoint. The production of microalgal extracts requires low-cost photobioreactors, minimal energy input, and potentially reducing feedstock expenditure [8]. The metal salts of microalgal nanoparticles are commercially available at relatively low costs compared to chemical-based nanoparticles [9], which require extreme processing temperatures, hazardous chemicals, and specialized equipment. However, nanoparticle synthesis using microalgal extracts works under ambient conditions, thereby significantly lowering both energy utilization and waste management costs [10].

With increasing demands for eco-friendly agricultural inputs, microalgae-derived nanoparticles present a promising opportunity to boost plant growth, control crop diseases, and aid in pollution remediation. However, comparative studies of these nanoparticles, particularly under field-relevant conditions and on staple crops are still limited, especially in regions like Pakistan, where affordable, effective and sustainable alternatives to conventional agrochemicals are urgently needed. This study focuses on synthesizing nanoparticles from the green microalgae Tetradesmus *nygardii* using salts of Ag, Ni, Cu, and Zn. We evaluate their biofertilizer efficiency in promoting tomato plant growth, antifungal activity against *Rhizopus* spp., and photocatalytic degradation of methylene blue dye under sunlight. This research aims to demonstrate the multifunctional potential of microalgal nanoparticles, supporting the transition towards greener, safer, and more accessible agricultural practices in regions burdened by chemical overuse.

2 | Methodology

2.1 | Microalgae Cultivation

The microalgae *Tetradesmus nygaardii* (strain no. MT858750) was obtained from the Environmental Microbiology lab at Quaid-i-Azam University, Islamabad, Pakistan. The strain was mass-cultivated in 15 L of Bold's Basal Medium (BBM) which contained KH_2PO_4 (17.5 g/100 mL), K_2HPO_4 (0.75 g/100 mL), $MgSO_4.H_2O$ (0.75 g/100 mL), NaCl (0.25 g/100 mL), $CaCl_2.2H_2O$ (0.25 g/100 mL), $NaNO_3$ (2.5 g/100 mL), EDTA (0.5 g/100 mL), H_3BO_3 (1.14 g/100 mL), KOH (3.1 g/100 mL), $FeSO_4.7H_2O$ (0.49 g/100 mL). Additionally, micronutrient solution composed of $ZnSO_4$ (0.441 g/50 ml), $MnCl_2.4H_2O$ (0.072 g/50 mL), $CuSO_4.5H_2O$ (0.078 g/50 mL), $CO(NO_3).6H_2O$ (0.024 g/50 mL) was added, and the medium was adjusted to pH 7.0. Cultivation was carried out in a photobioreactor at 25°C under continuous illumination (50 μmol photons/m_2/s), with aeration at a flow rate of 5 L/min using air pumps. After 21 days of growth, the biomass was harvested by centrifugation at 5000 rpm for 10 min and subsequently dried in a desiccator at 60°C for 48 h.

2.2 | Synthesis of Metal Oxide Nanoparticles From Microalgal Extract

The aqueous extract of dried microalgal biomass was prepared by suspending 1 g of biomass in 500 mL of distilled water and heating it in a water bath at 80°C for 24 hours. The extract was then filtered twice using Whatman filter paper No. 2. Metallic salt solutions of $NiSO_4$, $CuSO_4$, and $ZnSO_4$ were prepared at 0.15 M concentration, along with a 0.05 M solution of $AgNO_3$.

For nanoparticle synthesis, 500 mL of microalgal extract was individually mixed with each metallic salt solution and incubated at 25°C on a magnetic stirrer for 2 h, until a color change was observed. The reduction of metallic ions to produce nanoparticles was confirmed by UV-vis spectroscopy using a Spectra Max 190 microplate reader in the wavelength range from 200 to 1000 nm at a resolution of 1 nm, to identify characteristic peaks corresponding to each nanoparticle type. Beer–Lambert's law ($A = \varepsilon \cdot c \cdot l$) was used to estimate the concentration of nanoparticles in suspension. The mixtures were then centrifuged at 6000 rpm for 15 min to pellet the nanoparticles. The obtained nanoparticles were washed repeatedly with distilled water and dried in a desiccator at 60°C. Finally, the dried nanoparticles were calcinated in a furnace at 400°C for 2 h to convert them into their respective metal oxide nanoparticles: NiONPs (Nickel oxide), CuONPs (Copper oxide), ZnONPs (zinc oxide), and AgONPs (silver oxide).

2.3 | Characterization of the Biosynthesized Nanoparticles and Microalgal Biomass

The synthesized nanoparticles were characterized via Fourier Transformed Infrared Spectroscopy (FT-IR) and X-ray Diffraction (XRD). The surface functional groups present in both the microalgal biomass and the purified metal oxide nanoparticles were determined using FTIR spectroscopy. The measurements were conducted with a PerkinElmer FTIR spectrometer (Waltham, MA, USA) across a wave number range of 4000–400 cm^{-1}. The X-ray diffraction patterns were acquired using a Shimadzu XRD-6000 diffractometer with Cu Kα radiation ($\lambda = 1.5406$ Å) over a 2θ range of 20°–80°. Each sample was exposed for 300 s, with proper dark noise subtraction performed under identical measurement conditions. The obtained diffraction patterns were subjected to baseline correction using Origin software, followed by spectral deconvolution of energy peaks based on Gaussian distribution functions.

2.4 | Biofertilizer Potential of Microalgal-Derived Nanoparticles

The experiment was conducted in pots (3-inch size) containing 500 g of sterile soil, which was obtained from Go Organics Farm, Islamabad. Tomato (*Solanum lycopersicum*) was selected as the test crop due to its regional dietary importance and susceptibility to fungal pathogens. Commercial tomato seeds (legally approved for trade and commercialization in China) were purchased from the local market in Islamabad, Pakistan. Initially, seeds were soaked in distilled water for 24 h in the dark, then treated with 0.1% mercuric chloride for 3 min, and finally rinsed three times with sterilized distilled water. A total of seven treatments were applied: T1 (Negative control, soil only), T2 (Positive control, 1 g of microalgae), T3 (0.5 g of AgONP), T4 (0.5 g of CuONP), T5 (0.5 g of ZnONP), T6 (0.5 g of NiONP) and T7 (Combined effect of all nanoparticles, 0.1 g of each NP). The pots were maintained in the Biosciences Greenhouse facility at Quaid-i-Azam University, Islamabad, under controlled temperature conditions 24°C during the day and 20°C at night for plant growth. The soil in the pots was irrigated regularly to maintain 60% water holding capacity. Chlorophyll content in the plants was measured using a SPAD meter. After harvesting, plant biometric analysis was performed, and assessment of disease prevalence was recorded using the following formula:

Disease Prevalence (%) = (Number of diseased leaves/Total number of leaves) × 100.

Soil pH and electrical conductivity (EC) were measured using a calibrated digital multimeter. Prior to measurements, the meters were calibrated using standard buffer solutions of pH 4.0, 7.0 and 10.0 and 1413 μS/cm standard solution was used for EC calibration. For each pot, three soil samples were collected. Chlorophyll content was measured using a SPAD-502 meter, which was calibrated according to the manufacturer's instructions before use. All measurements were recorded in triplicate across three biological replicates per treatment.

2.5 | Antifungal Assay

The antifungal activity of the synthesized nanoparticles was evaluated against *Rhizopus* spp. (NCBI Taxonomy ID: 145392, accession number: MT497471.1). The fungal strain was identified and obtained from the Department of Microbiology, Quaid-i-Azam University, Islamabad, Pakistan. Fungal isolates were cultured and maintained on potato dextrose agar (PDA) and stored at 4°C or sub-cultured monthly for further use. The antifungal activity of the microalgae-derived nanoparticles was assessed using the poisoned food technique [11]. This method was used to determine the percentage of mycelial growth inhibition, the minimum inhibitory concentration (MIC), and the minimum fungicidal concentration (MFC) of each nanoparticle. The MIC and MFC were estimated using the formulas:

% Inhibition = [(dc − dt)/dc] × 100.

A stock suspension of each nanoparticle was prepared at a concentration of 200 μg/mL in distilled water. Serial dilutions were then performed to obtain working concentrations of 150, 100, and 50 μg/mL, corresponding to 75%, 50%, and 25% of the stock concentration, respectively. Briefly, 1 mL of each nanoparticle suspension at each concentration was aseptically poured into sterile petri dishes, followed by the addition of 15 mL of molten potato dextrose agar (PDA). After solidification, a 5 mm diameter mycelial disc, obtained from a 7-day-old pure *Rhizopus* culture, was aseptically placed at the center of each plate. Plates were then incubated at 25°C for 7 days. Control plates containing PDA without nanoparticles were used for comparison. Antifungal efficacy was assessed by measuring the radial growth of the fungal colonies and calculating the percentage of growth inhibition.

2.6 | Photocatalytic Potential of the Biosynthesized Nanoparticles

The photocatalytic activity of NiONPs, CuONPs, ZnONPs, and AgONPs was assessed using the degradation of methylene blue (MB) dye as a model pollutant at an initial concentration of 10 mg/L. The efficiency of dye degradation was calculated using the formula:

$$\text{Degradation Efficiency} = \frac{Co - Ct}{Co} \times 100$$

where C_o is the initial absorbance of the dye and C_t is the absorbance at time t, measured at 665 nm.

For each treatment, 50 mL of the dye solution was transferred into a separate beaker, and 60 mg of the respective nanoparticles were added, giving a catalyst dosage of 1.2 g/L. A control containing MB dye without any nanoparticles was maintained to account for photolysis. Prior to sunlight exposure, the nanoparticle-dye mixtures were sonicated in the dark for 15 min to ensure uniform dispersion of the nanoparticles. Subsequently, the beakers were exposed to direct sunlight in a glasshouse between 11:00 AM and 3:00 PM under clear weather conditions. Based on regional solar radiation data for Islamabad and standard clear-sky conditions, the solar irradiance during the experimental period was estimated to be in the range of 700–900 W/m^2, corresponding to peak daytime solar intensity. Samples were collected at 2-hour and 4-hour intervals by pipetting 2 mL aliquots into Eppendorf tubes, followed by centrifugation at 10,000 rpm for 10 min. The supernatant was then analyzed using a UV-Vis spectrophotometer at 664 nm to determine the extent of MB dye degradation, indicating the photocatalytic efficiency of each nanoparticle.

To evaluate degradation kinetics, the experimental data were fitted to a pseudo-first-order kinetic model, expressed as:

$$In(Ct/Co) = -kt$$

2.7 | Statistical Analysis

All experiments were conducted in triplicate, and results were analyzed statistically as average replicates. The mean and the standard deviation of the growth parameters were calculated with Microsoft Excel. The differences between various treatments were analyzed using one-way ANOVA. A p-value of less than 0.05 was considered significant.

3 | Results and Discussion

3.1 | Synthesis and Characterization of Metal Oxide Nanoparticles

3.1.1 | UV–Visible Spectroscopy Analysis

The biosynthesis of all metal oxide nanoparticles using microalgal extract was initially confirmed by UV–Visible spectroscopy (Figure 1). Each nanoparticle exhibited a distinct absorbance peak corresponding to surface plasmon resonance, confirming the formation of nanoparticles. Specifically, NiONPs showed a primary absorbance peak at 360 nm, consistent with previous reports on nickel oxide nanoparticles [12]. CuONPs at 290 nm, ZnONPs at 370 nm, and AgONPs at 430 nm, all of which align with the reported values for their respective metal oxide nanoparticles [5, 6, 13]. These characteristic peaks demonstrate the optical activity of each nanoparticle. Furthermore, the variation in peak positions reflects differences in unique electronic transitions and size-related quantum effects, supporting the distinct physicochemical identities of each nanoparticle type.

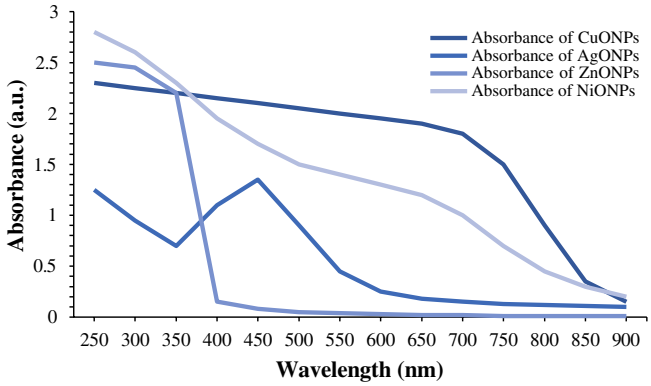

FIGURE 1 | UV-spectroscopy of metal oxide nanoparticles.

The color change observed during the synthesis indicated the formation of nanoparticles from nickel sulfate, copper sulfate, zinc sulfate, and silver nitrate precursors. Specifically, nickel sulfate and copper sulfate nanoparticles exhibited a color change to bluish-green, zinc sulfate nanoparticles turned brown, while silver nitrate nanoparticles changed to black. UV-visible spectroscopy was performed prior to calcination to confirm the initial bio-reduction of metal ions by the microalgal extracts, representing the intermediate zero-valent nanoparticle stage of the synthesis process. Nickel sulfate nanoparticles showed a secondary absorption peak observed near 450 nm, attributed to d-d electronic transitions of residual Ni^2 ions within the oxide lattice prior to complete calcination [14]. The 360 nm peak is therefore considered the definitive absorbance maximum for the fully formed NiONPs. Copper and zinc sulfate nanoparticles exhibited a characteristic peak at 350 nm, indicative of Cu^{2+} and Zn^{2+} as reported by [15, 16], respectively. For silver nitrate nanoparticles, a strong absorption peak at 400 nm was observed, consistent with the reduction of Ag^+ [17]. These spectroscopic features collectively confirm the successful bio-reduction of metal ions as an intermediate step to their corresponding zero-valent nanoparticle states.

3.1.2 | Fourier Transform Infrared Spectrophotometric Analysis

FTIR analysis was conducted to identify the functional groups involved in the reduction and stabilization of the synthesized metal oxide nanoparticles using the microalgal extract. Spectra were recorded for both the microalgal extract and the nanoparticles. In the algal extract, broad absorption peaks observed around 3280 cm^{-1} were attributed to O—H and N—H stretching vibrations, indicating the presence of phenolic and amine groups. Peaks near 1640 cm^{-1} corresponded to C═O stretching (amide I), while bands at 1384 and 1040 cm^{-1} were assigned to C—H bending and C—O—C stretching, respectively. Upon nanoparticle synthesis, shifts in these peaks were observed in all samples, confirming the involvement of algal biomolecules in capping and stabilizing the nanoparticles. Specifically, each nanoparticle exhibited distinctive absorption bands indicating successful bio-reduction and formation of metal oxides. NiONPs showed strong O—H stretching bands at 3701.75 and 3648.03 cm^{-1}, attributed to hydroxyl groups of surface-adsorbed

water and phenolic compounds present in the algal extract. The absorption at 3204.56 cm^{-1} is assigned to N—H stretching of amide groups from algal proteins. A distinctive absorption band in the range of 400–600 cm^{-1} confirms Ni—O stretching vibrations, validating the formation of NiONPs (Figure 2). CuONPs presented O—H stretching bands at 3701.39 and 3648.40 cm^{-1}, consistent with hydroxyl and phenolic functionalities from the algal biomass. The absorption at 3141.66 cm^{-1} is assigned to N—H stretching of amine groups in algal proteins. The band at 2050.56 cm^{-1} previously assigned to allene stretching is more appropriately attributed to asymmetric stretching of carboxylate groups, which is commonly observed in biosynthesized metal oxide nanoparticles (Figure 2). ZnONPs showed O—H stretching bands at 3779.39 and 3648.40 cm^{-1}, attributed to surface hydroxyl groups and phenolic compounds. The absorption at 3141.66 cm^{-1} is assigned to N—H stretching of protein-derived amine groups. The band at 2050.56 cm^{-1} is assigned to adsorbed carboxylate stretching. The C═O stretching at 1683.82 cm^{-1} corresponds to amide I vibrations of algal proteins involved in nanoparticle stabilization (Figure 2). AgONPs were characterized by N—H stretching at 3374.39 cm^{-1}, attributed to aliphatic amine groups of algal proteins. The band at 2340.40 cm^{-1} corresponds to CO_2 adsorbed on the nanoparticle surface. C—H bending at 1763.66 cm^{-1} and C═O stretching at 1743.82 cm^{-1} are attributed to carbonyl groups of algal lipids and proteins involved in surface stabilization of aromatic compounds. S═O stretching at 1371.56 cm^{-1} is consistent with sulfoxide groups present in algal biomolecules (Figure 2). Moreover, all nanoparticles exhibited new absorption bands in the range of 400–600 cm^{1}, corresponding to metal–oxygen (M–O) stretching vibrations, which confirms the formation of the respective metal oxides. These observations collectively validate the bio-reduction of metal salts and stabilization of nanoparticles by bioactive functional groups present in the algal extract.

3.1.3 | X-Ray Diffraction

X-ray diffraction (XRD) analysis was carried out to investigate the crystalline structure and estimate the average crystallite size of the biosynthesized nanoparticles. Distinct diffraction peaks were observed for each type of metal oxide nanoparticle, confirming successful synthesis and crystallinity. The average crystallite size (D) was calculated using the Scherrer equation:

$$D = \frac{K\lambda}{\beta\theta}$$

where

- D = crystallite size (nm)
- K = shape factor (0.9)
- λ = X-ray wavelength
- β = full width at half maximum (FWHM) in radians
- θ = Bragg angle (in radians)

The XRD pattern of NiONPs exhibited sharp diffraction peaks at 2θ = 20.69° with lower intensity peaks at 33.04° and 38.30°, indexed to the (101), (110) and (111) corresponding to the characteristic planes of face-centered cubic NiO, in agreement with JCPDS card No. 47-1049. The calculated crystallite sizes were 11.8, 18.9, and 18.7 nm, respectively, indicating well-formed nanocrystalline domains (Figure 3a). The XRD pattern of CuONPs showed multiple diffraction peaks distributed across the 20°–80° range, with prominent reflections at 2θ values of 31.27°, 35.47°, and 38.71°, indexed to the (110), (002), and (111) planes of monoclinic CuO, consistent with JCPDS card No. 45-0937. The corresponding crystallite sizes were calculated as 11.2, 12.2, and 13.9 nm, demonstrating a narrow size distribution and uniform particle morphology (Figure 3b).

In contrast, the XRD pattern of AgONPs displayed broader peaks at 2θ values of 23.59°, 38.29°, and 44.65°, indexed to the (110), (111) and (200) planes of cubic AgO2, consistent with JCPDS card No. 41-1104. The calculated ultra-small crystallite sizes of 2.70, 1.23, and 1.54 nm confirm the formation of ultra-fine nanoparticles with a high surface area-to-volume ratio (Figure 3c). This exceptionally small size is attributed to the high concentration of bioactive capping molecules present in the microalgal extract, which adsorb onto nucleating Ag2O crystal surfaces, effectively limiting crystal growth during the synthesis process. These results confirm the successful synthesis of phase-pure, crystalline metal oxide nanoparticles using *Tetradesmus nygaardii* extract. Among all synthesized nanoparticles, AgONPs exhibited the smallest crystallite size, which is strongly associated with enhanced surface energy and reactivity. These physicochemical characteristics likely contributed to their superior performance observed in subsequent applications, including biofertilizer efficacy, antifungal activity, and photocatalytic degradation.

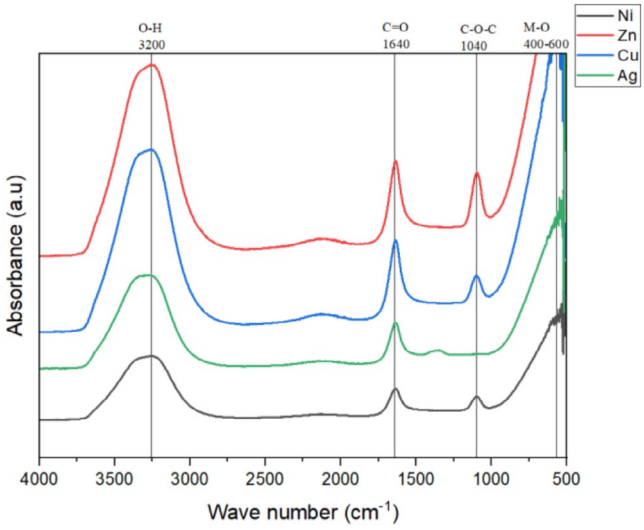

FIGURE 2 | FTIR spectral analysis of metal oxide nanoparticles.

3.2 | Biofertilizer Efficacy of Nanoparticles on Tomato Plants

3.2.1 | Plant Biometrical Parameters

Substantial variations were observed in root and shoot development across treatments. The combined nanoparticle treatment produced the longest roots and shoots (Figure 4a,b), followed by

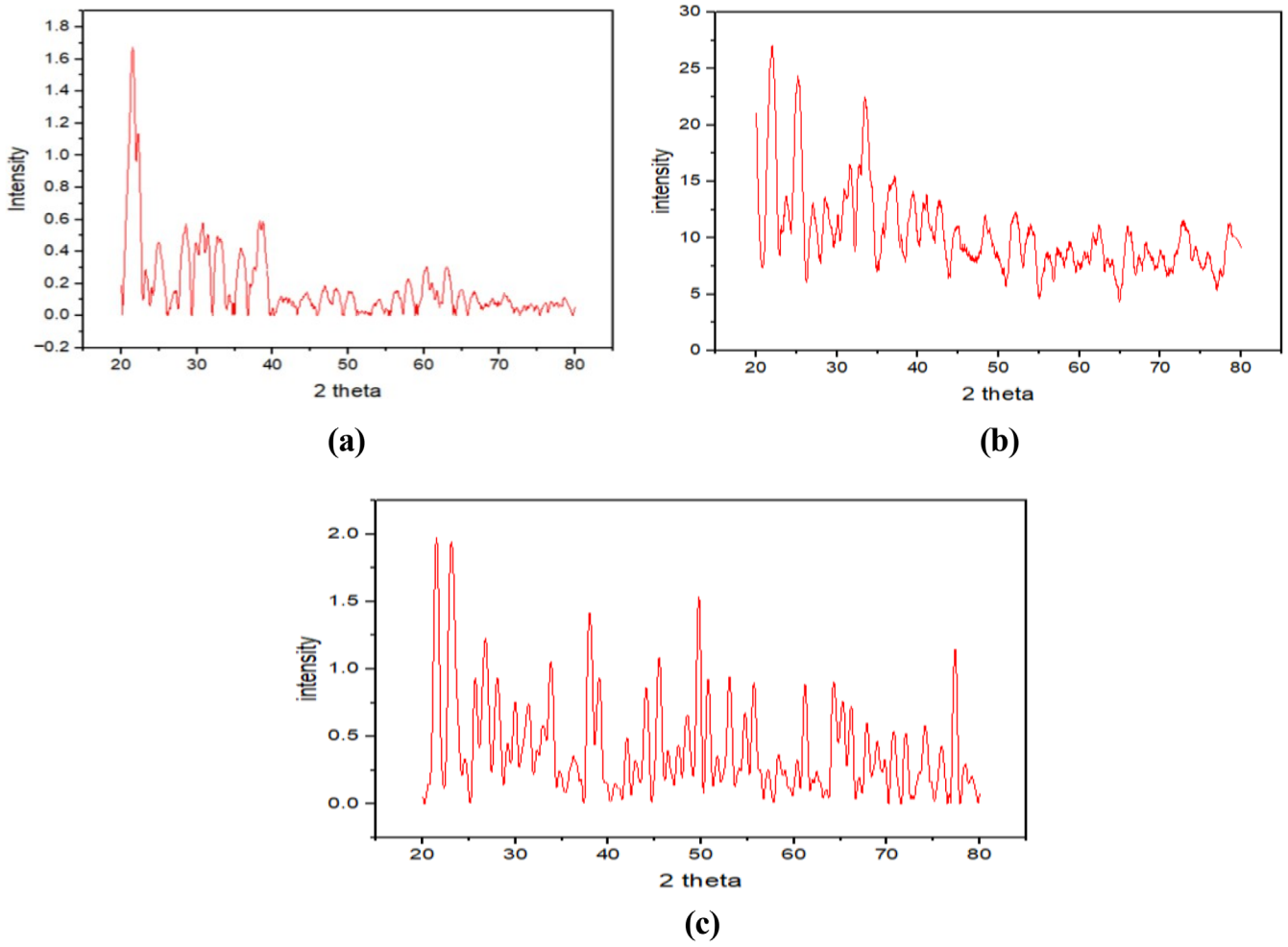

FIGURE 3 | XRD spectra of biologically synthesized metal oxide nanoparticles (a) NiONPs, (b) CuONPs and (c) AgONPs.

AgONPs alone, highlighting their effectiveness in modulating plant hormone signaling pathways, particularly auxin-mediated root elongation, thereby stimulating lateral root formation and biomass accumulation. NiONPs and CuONPs, as essential micronutrient sources, may enhance enzymatic activity associated with nitrogen assimilation, contributing to moderate growth improvements observed under these treatments. In contrast, ZnONPs resulted in stunted growth, possibly due to excessive Zn^{2+} ion release. AgONPs-treated plants recorded high fresh shoot and root weights (Figure 4c,d). Notably, the combined treatment surpassed individual treatments in shoot weight, suggesting cumulative or additive effects. ZnONPs-treated plants consistently displayed the lowest biomass, reinforcing their phytotoxic impact under the tested conditions.

The root scans of the tomato plant are depicted in Figure 5. Root architecture varied significantly across treatments. Control plants exhibited a normal root system, which served as the reference baseline. Plants treated with microalgae demonstrated enhanced elongation and increased lateral branching, suggesting that metabolites secreted by microalgae may act as natural growth stimulators. Exposure to NiONPs and CuONPs also promoted root proliferation, indicating that at the applied concentrations, these nanoparticles may have contributed to improved nutrient availability or signaling pathways that favor root development. In contrast, ZnONPs markedly suppressed root density and elongation, reflecting a potential inhibitory effect on nutrient absorption within the root tissues. AgONPs, however, substantially increased root elongation and branching, which could be attributed to their antimicrobial properties, reducing rhizospheric stress and indirectly favoring root expansion. The most pronounced effect was observed with the combined application of NiONPs, CuONPs, ZnONPs, and AgONPs, where roots exhibited a highly branched and dense architecture. This synergistic enhancement suggests that, despite the inhibitory effects of ZnONPs alone, their interaction with other nanoparticles may offset individual limitations and collectively stimulate root system development.

3.2.2 | Chlorophyll Content and Photosynthetic Activity

The application of biosynthesized metal oxide nanoparticles significantly influenced chlorophyll content in tomato plants, as measured by SPAD (Soil Plant Analysis Development) values. Among all treatments, AgONPs yielded the highest SPAD readings, ranging between 33.7 and 37.8 μmol m^{-2}, surpassing both the microalgal control (MAC: 21.3–23.4 μmol m^{-2}) and untreated control (10–15.2 μmol m^{-2}). The substantial increase in chlorophyll content under AgONP treatment is likely mediated through enhanced nitrogen and magnesium availability within the rhizosphere, both of which are

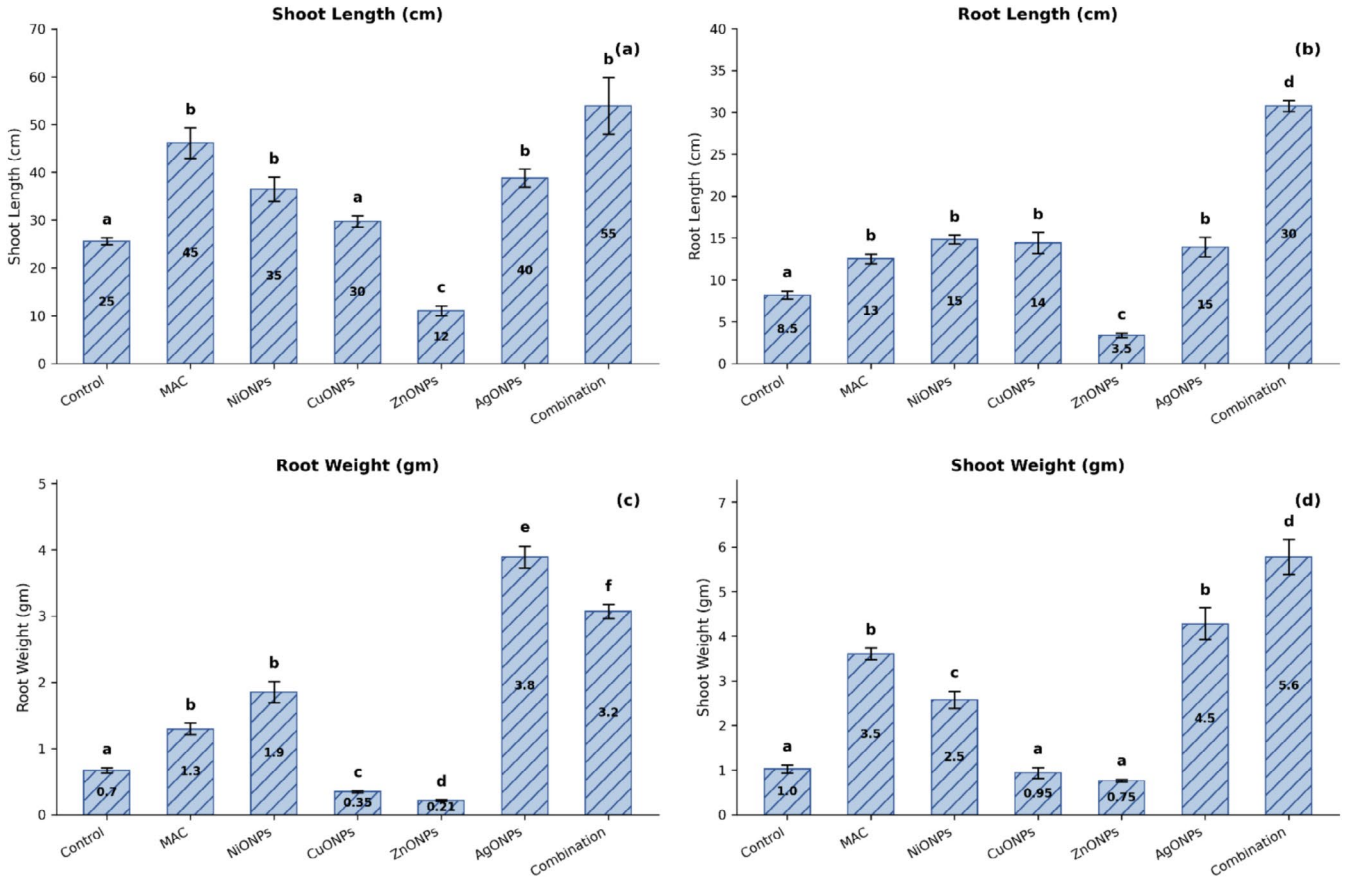

FIGURE 4 | Length and weight of the root and shoot: (a) shoot length (cm), (b) root length (cm), (c) root weight (gm), shoot weight (gm).

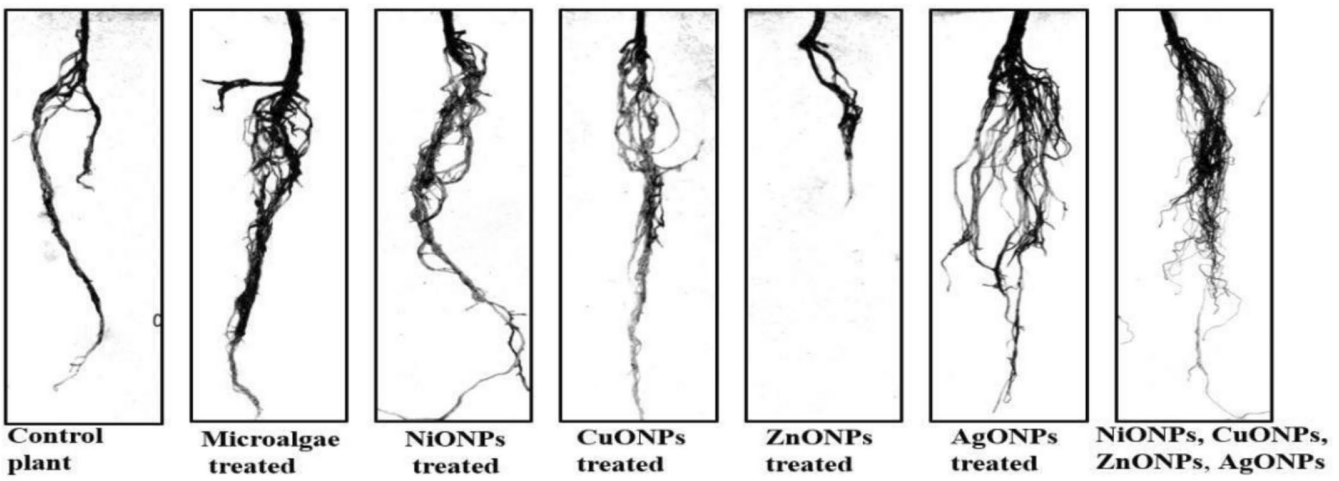

FIGURE 5 | Root scans of the tomato plant with the treatment of microalgae-mediated metal oxide nanoparticles.

essential components of the chlorophyll molecule. The treatment combining all four nanoparticles also produced comparable chlorophyll levels (31.6–38.4 μmol m^{-2}) (Figure 6), suggesting synergistic interactions that favor photosynthetic pigment synthesis. NiONPs and CuONPs demonstrated moderate improvements, with SPAD ranges of 23.8–34.1 μmol m^{-2} and 26–32.3 μmol m^{-2}, respectively. In contrast, ZnONPs showed minimal effect, indicating limited or potentially inhibitory influence on chlorophyll biosynthesis when applied independently.

3.3 | Disease Incidence and Antifungal Effects

To accurately assess the impact of nanoparticle treatments on plant health, both the total number of leaves per plant (Figure 7a) and the number of diseased leaves (Figure 7b) were quantified. Among the treatments, plants exposed to ZnONPs produced the lowest total number of leaves, which may reflect growth inhibition or phytotoxic effects of excess zinc. In contrast, AgONPs and the combined nanoparticle treatment supported the highest leaf numbers, suggesting that silver's bioactivity and potential

synergistic effects of the metal oxides not only reduced disease pressure but also promoted overall plant growth. A significant reduction in fungal disease incidence was noted in nanoparticle-treated groups. Plants treated with AgONPs exhibited the lowest disease prevalence (3.03%), followed by those receiving the combined NP treatment (6.25%) and NiONPs (12.5%), while untreated controls exhibited a disease incidence of 38.46%. The reduction in fungal disease prevalence observed under AgONP treatment is consistent with the broad-spectrum antimicrobial mechanism of silver, which involves the disruption of fungal cell membrane integrity through direct Ag^{+} ion interaction with thiol groups of membrane-associated proteins, inhibition of respiratory enzymes, collectively leading to fungal cell death. Conversely, ZnONPs treated plants had the highest disease incidence (50%) (Figure 7c), indicating their limited effectiveness in inhibiting phytopathogens, possibly due to ionic toxicity or insufficient antifungal activity. These findings strongly suggest that AgONPs possess potent antifungal properties, supporting previous reports on silver's broad-spectrum antimicrobial [6]. The relatively low disease rate of the combined treatment suggests that metal oxide synergy can offer enhanced disease suppression.

3.4 | Effects on Soil Properties

In addition to plant growth metrics, changes in soil pH and electrical conductivity (EC) were analyzed to evaluate the effect of treatment on soil health. All treatments resulted in a slight increase in soil pH above the initial value of 7.6. AgONPs and the control group exhibited similar alkaline readings (~8.14), while NiONPs maintained a comparatively moderate pH of 7.98 (Figure 8). This near-neutral condition is considered more favorable for rhizospheric processes, as excessive alkalinity can reduce the solubility and availability of essential micronutrients, thereby constraining uptake. EC values declined markedly across most treatments relative to the baseline of 4000 µS/cm. The greatest reductions were recorded in CuONPs (664 µS/cm), NiONPs (870 µS/cm), and the combined treatment (910 µS/cm), reflecting reduced soil salinity and an improved ionic balance. Such reductions are likely to have mitigated osmotic stress, creating conditions that are conducive to enhanced water and nutrient absorption, which is consistent with the improved growth performance observed under these treatments. Conversely, ZnONPs-treated soils retained a comparatively high EC (3400 µS/cm), suggesting persistence of soluble salts

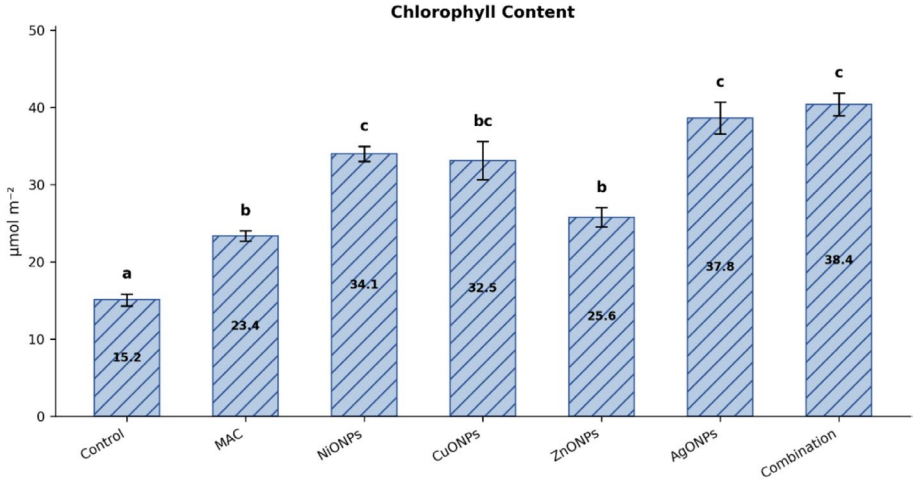

FIGURE 6 | Chlorophyll content of the tomato plant under different treatments.

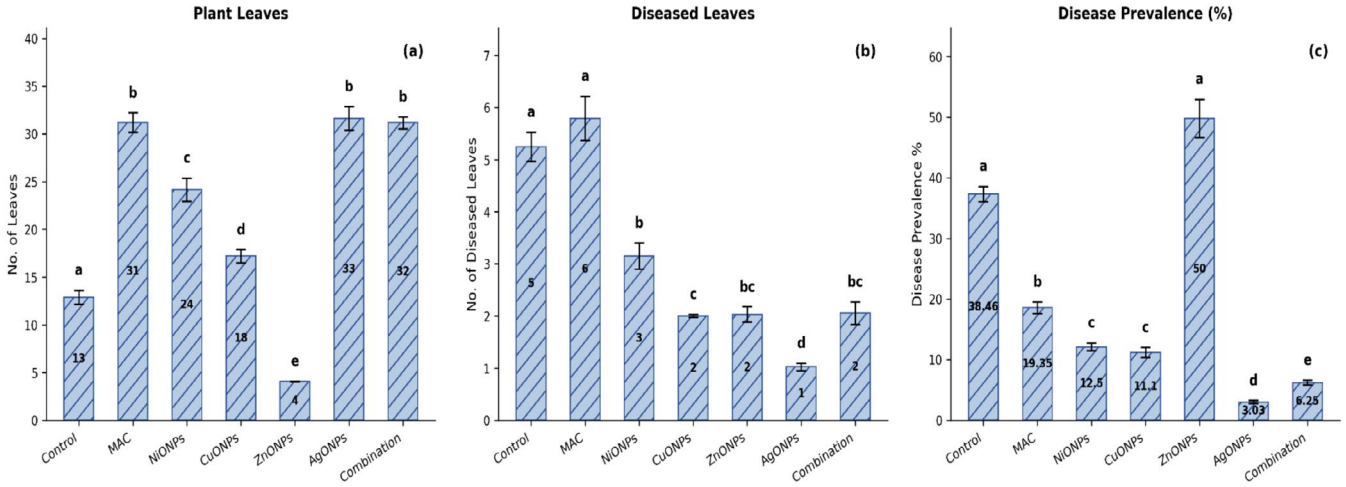

FIGURE 7 | Disease incidence in the tomato plant under varying treatment effects; (a) total no of leaves, (b) total no of diseased leaves, (c) disease prevalence percentage.

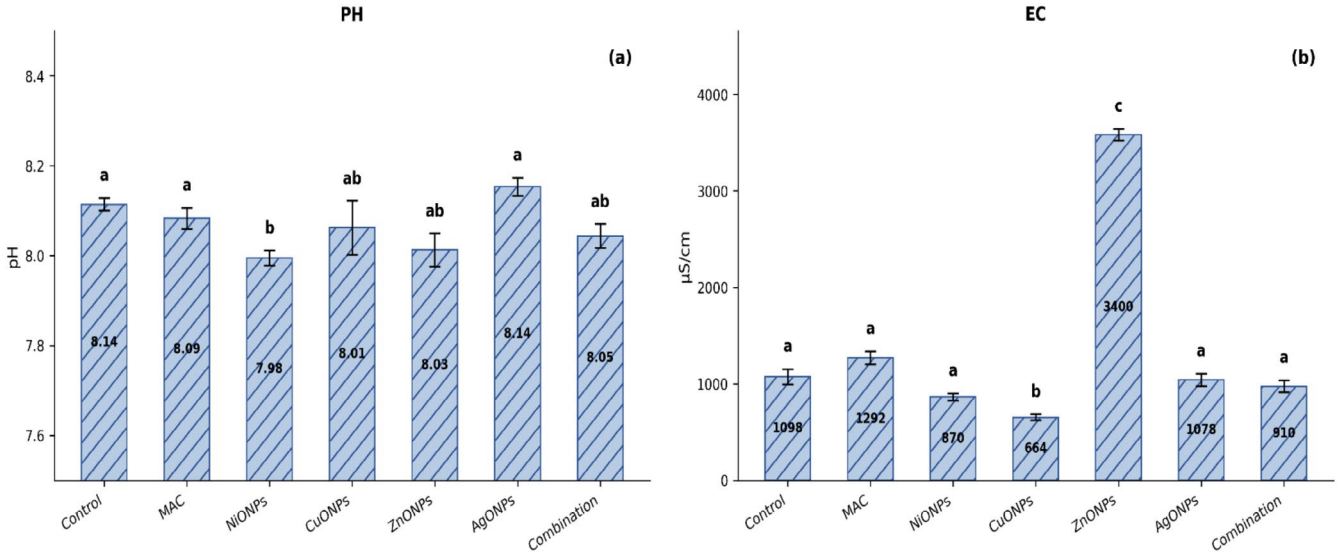

FIGURE 8 | Effect on the soil properties of the tomato plants treated with metal oxide nanoparticles; (a) pH, (b) EC.

and potential ionic toxicity. This elevated salinity can impose osmotic pressure on roots, restricting water uptake and contributing to the comparatively reduced plant performance observed in this group.

3.5 | Antifungal Activity of Synthesized Nanoparticles

The antifungal potential of microalgae-mediated metal oxide nanoparticles was assessed using the poisoned food technique against *Rhizopus* spp., a common phytopathogenic fungus. All nanoparticle treatments demonstrated a clear dose-dependent inhibition of fungal mycelial growth, with varying degrees of effectiveness.

3.5.1 | Mycelial Growth Inhibition Patterns

All nanoparticles exhibited clear dose-dependent inhibition of *Rhizopus* growth, with complete suppression observed at 200 µg/mL. NiONPs reduced colony diameter from 8 cm at 50 µg/mL to 4 cm at 100 µg/mL and further to 1 cm at 150 µg/mL, achieving total inhibition at 200 µg/mL. CuONPs displayed a similar pattern, with colony diameters of 4 cm and 3.5 cm at 100 and 150 µg/mL, respectively, and full inhibition at 200 µg/mL. ZnONPs showed stronger mycelial growth limitation at intermediate doses, with colony diameters of 3 cm at 100 µg/mL and 2 cm at 150 µg/mL, followed by complete suppression at 200 µg/mL. AgONPs showed a comparatively delayed inhibitory effect, with colony sizes of 6, 5, and 3 cm at 50, 100, and 150 µg/mL, respectively, reaching full inhibition only at 200 µg/mL (Figure 9). These differential responses likely reflect distinct but overlapping antifungal mechanisms: the early potency of NiONPs may be due to rapid reactive oxygen species (ROS) generation and Ni^{2+}-mediated disruption of fungal metabolism; ZnONP's pronounced effects at intermediate doses are consistent with partial dissolution to Zn^{2+} and strong interactions with fungal cell walls and membranes; CuONPs likely exert their effects through redox reactions and binding to thiol groups in fungal proteins; whereas AgONPs primarily disrupt membrane lipids and increase membrane permeability, potentially requiring higher slower ion-release kinetics to achieve complete fungicidal action. Overall, ion release, oxidative stress, and membrane perturbation appear to underlie the dose-dependent antifungal activity observed [18].

3.6 | Photocatalytic Activity of Metal Oxide Nanoparticles

The photocatalytic activity of biosynthesized metal oxide nanoparticles was evaluated through the degradation of methylene blue (MB) dye under natural sunlight over a period of 4 h. Among all treatments, AgONPs demonstrated the highest photocatalytic performance, achieving 98.27% degradation with a degradation rate of 30.84% per hour. This enhanced performance is likely attributed to their ultra-small crystallite size, as confirmed by XRD, which offers a high surface area-to-volume ratio and facilitates effective charge carrier separation. These properties enable greater interaction with light and more efficient generation of ROS, including hydroxyl and superoxide radicals, which accelerate dye breakdown. ZnONPs also exhibited notable photocatalytic activity with a degradation efficiency of 97.06% and a rate of 6.65% per hour. Their efficacy may be linked to their wide band gap and strong ability to absorb UV radiation, coupled with their surface chemistry that promotes ROS formation. NiONPs followed closely, degrading 92.80% of MB dye with a rate of 22.06% per hour. Their catalytic activity can be attributed to their redox-active nature, which facilitates electron transfer and delays recombination of photogenerated charge carriers. In contrast, CuONPs showed significantly lower performance, with only 19.62% degradation and a rate of 3.58% per hour, possibly due to higher rates of electron-hole recombination and lower band gap alignment with the solar spectrum, limiting their ability to generate sufficient ROS. The control sample, which contained MB dye without any nanoparticles, exhibited negligible degradation under sunlight, confirming that the observed photodegradation was primarily driven by the photocatalytic action of the nanoparticles. These findings underscore

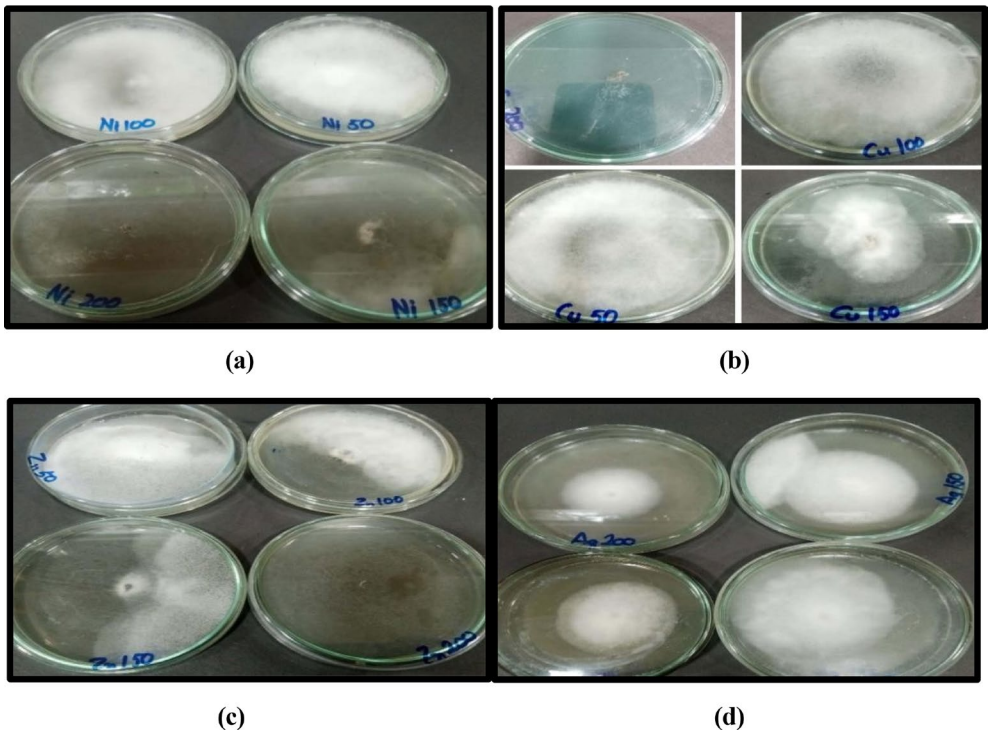

FIGURE 9 | Antifungal activity of metal oxide nanoparticles against fungal mycelial growth. (a) NiONPs. (b) CuONPs. (c) ZnONPs. (d) AgONPs.

TABLE 1 | Optical density values of MB dye after 2 h and 4 h of treatment with nanoparticles, degradation rate per hour, and total degradation percentage of the MB dye.

Nanoparticles	OD value after 2 h	OD value after 4 h	Degradation rate (% per hour)	Percentage degradation
NiONPs	1.38	0.19	22.06	92.80
CuONPs	2.32	2.13	3.58	19.62
ZnONPs	0.43	0.078	6.65	97.06
AgONPs	1.68	0.046	30.84	98.27

the potential of biosynthesized AgONPs and ZnONPs as highly efficient, sunlight-driven photocatalysts for the treatment of organic pollutants, offering a green and sustainable approach for environmental remediation.

The photocatalytic degradation kinetics were further analyzed using a pseudo-first-order model. The linear relationship between $\ln(C_o/C_t)$ and irradiation time confirmed that the degradation process follows pseudo-first-order kinetics. The calculated rate constants (k) revealed that AgONPs exhibited the highest reaction rate ($k = 1.02\,h^{-1}$), followed by ZnONPs ($0.88\,h^{-1}$) and NiONPs ($0.66\,h^{-1}$), while CuONPs showed a significantly lower rate constant ($0.055\,h^{-1}$). This trend is in strong agreement with the observed degradation efficiencies, further validating the superior photocatalytic performance of AgONPs.

As shown in Table 1, the initial absorbance of MB dye decreased markedly in the presence of AgONPs, dropping from 1.68 at 2 h to 0.046 at 4 h, representing the most pronounced decline among all treatments. Similarly, ZnONPs reduced optical density (OD) from 0.43 to 0.078, highlighting their strong dye-removal capacity despite a comparatively lower degradation rate per hour. NiONPs also showed a sharp decline in OD values, from 1.38 at 2 h to 0.19 at 4 h, correlating well with their high overall degradation percentage. In contrast, CuONPs exhibited only a minor reduction in OD (2.32–2.13), indicating limited photocatalytic efficiency. These variations in OD correspond closely with the calculated degradation efficiencies and rates, providing a clear quantitative representation of the photocatalytic potential of each nanoparticle type. The consistency between OD decline, degradation rate, and overall percentage degradation not only validates the observed photocatalytic trends but also emphasizes the superior efficiency of AgONPs and ZnONPs in driving dye degradation under solar irradiation.

4 | Conclusion

This study successfully demonstrated the green synthesis of metal oxide nanoparticles using the microalgal extract of *Tetradesmus nygardii*. The biosynthesized nanoparticles exhibited distinct optical and structural characteristics, with AgONPs showing the smallest crystallite sizes, suggesting superior surface reactivity. The environmental applications of these nanoparticles were evaluated through their performance as biofertilizers, antifungal agents, and photocatalysts. Among

the tested nanoparticles, AgONPs consistently showed the most promising results across all applications, achieving the highest photocatalytic degradation efficiency of methylene blue dye under solar irradiation and the most substantial enhancement of plant productivity. ZnONPs were particularly effective in antifungal assays, while NiONPs exhibited substantial bioactivity in both plant growth and photocatalytic activity. CuONPs, while moderately effective, showed comparatively lower performance in photocatalysis and plant growth promotion. The findings suggest the potential of microalgae-based metal oxide nanoparticles as multifunctional agents in sustainable agriculture and environmental remediation. Their dual role in enhancing plant productivity and mitigating biotic and abiotic stresses suggests that these green-engineered nanoparticles can serve as viable substitutes for synthetic fertilizers, fungicides, and chemical catalysts.

Acknowledgments

Open Access funding enabled and organized by Projekt DEAL. [Correction added on 20 May 2026, after first online publication: Projekt DEAL funding statement has been added.]

Conflicts of Interest

The authors declare no conflicts of interest.

Data Availability Statement

Data sharing not applicable to this article as no datasets were generated or analysed during the current study.

References

1. A. Kiyani, S. Jamil, M. Hamayun, R. Abid, A. Jamal, and M. I. Ali, "Assessing the Synergistic Effect of *Chlorella vulgaris*, Seaweed and Inorganic Fertilizer for Enhancing Wheat Growth," *Pakistan Journal of Botany* 57, no. 4 (2025): 1323–1332, https://doi.org/10.30848/PJB2025-4(1).

2. A. Glass, "Nitrogen Use Efficiency of Crop Plants: Physiological Constraints Upon Nitrogen Absorption," *Critical Reviews in Plant Sciences* 22, no. 5 (2003): 453–470, https://doi.org/10.1080/713989757.

3. F. Ma, Y. Li, X. Han, et al., "Microalgae-Based Biofertilizer Improves Fruit Yield and Controls Greenhouse Gas Emissions in a Hawthorn Orchard," *PLoS One* 19, no. 8 (2024): e0307774, https://doi.org/10.1371/journal.pone.0307774.

4. X. Song, J. Liu, Y. Feng, et al., "Microalgae-Based Biofertilizers Improve Fertility and Microbial Community Structures in the Soil of Potted Tomato," *Frontiers in Plant Science* 15 (2024): 1461945, https://doi.org/10.3389/fpls.2024.1461945.

5. T. S. Aldeen, H. E. A. Mohamed, and M. Maaza, "ZnO Nanoparticles Prepared via a Green Synthesis Approach: Physical Properties, Photocatalytic and Antibacterial Activity," *Journal of Physics and Chemistry of Solids* 160 (2022): 110313, https://doi.org/10.1016/j.jpcs.2021.110313.

6. L. Castillo-Henríquez, K. Alfaro-Aguilar, J. Ugalde-álvarez, et al., "Green Synthesis of Gold and Silver Nanoparticles From Plant Extracts and Their Possible Applications as Antimicrobial Agents in the Agricultural Area," *Nanomaterials* 10, no. 9 (2020): 1–24, https://doi.org/10.3390/nano10091763.

7. S. Uddin, L. B. Safdar, J. Iqbal, et al., "Green Synthesis of Nickel Oxide Nanoparticles Using Leaf Extract of Berberis balochistanica: Characterization, and Diverse Biological Applications," *Microscopy Research and Technique* 84, no. 9 (2021): 2004–2016.

8. V. K. Garlapati, S. Sharma, D. Sharma, et al., "Sustainable Production of Microalgal Nanoparticles Through Green Synthesis Towards Cancer Treatment," *Frontiers in Bioengineering and Biotechnology* 13 (2025): 1621876, https://doi.org/10.3389/fbioe.2025.1621876.

9. J. M. Jacob, R. Ravindran, M. Narayanan, S. M. Samuel, A. Pugazhendhi, and G. Kumar, "Microalgae: A Prospective Low Cost Green Alternative for Nanoparticle Synthesis," *Current Opinion in Environmental Science & Health* 20 (2021): 100163, https://doi.org/10.1016/j.coesh.2019.12.005.

10. S. Choudhary, G. Kumawat, M. Khandelwal, et al., "Phyco-Synthesis of Silver Nanoparticles by Environmentally Safe Approach and Their Applications," *Scientific Reports* 14, no. 1 (2024): 9568, https://doi.org/10.1038/s41598-024-60195-3.

11. M. M. Gakuubi, A. W. Maina, and J. M. Wagacha, "Antifungal Activity of Essential Oil of *Eucalyptus camaldulensis* Dehnh. Against Selected Fusarium Spp," *International Journal of Microbiology* 2017, no. 1 (2017): 8761610, https://doi.org/10.1155/2017/8761610.

12. S. Uddin, L. B. Safdar, S. Anwar, et al., "Green Synthesis of Nickel Oxide Nanoparticles From Berberis balochistanica Stem for Investigating Bioactivities," *Molecules* 26, no. 6 (2021): 1548.

13. T. Gur, I. Meydan, H. Seckin, M. Bekmezci, and F. Sen, "Green Synthesis, Characterization and Bioactivity of Biogenic Zinc Oxide Nanoparticles," *Environmental Research* 204 (2022): 111897, https://doi.org/10.1016/J.ENVRES.2021.111897.

14. S. P. Chandran, M. Chaudhary, R. Pasricha, A. Ahmad, and M. Sastry, "Synthesis of Gold Nanotriangles and Silver Nanoparticles Using *Aloe vera* Plant Extract," *Biotechnology Progress* 22, no. 2 (2006): 577–583, https://doi.org/10.1021/bp0501423.

15. A. A. Barzinjy and H. H. Azeez, "Green Synthesis and Characterization of Zinc Oxide Nanoparticles Using *Eucalyptus globulus* Labill. Leaf Extract and Zinc Nitrate Hexahydrate Salt," *SN Applied Sciences* 2, no. 5 (2020): 991.

16. K. M. Rajesh, B. Ajitha, Y. A. K. Reddy, Y. Suneetha, and P. S. Reddy, "Assisted Green Synthesis of Copper Nanoparticles Using *Syzygium aromaticum* Bud Extract: Physical, Optical and Antimicrobial Properties," *Optik* 154 (2018): 593–600, https://doi.org/10.1016/j.ijleo.2017.10.074.

17. V. C. Gosavi, A. A. Daspute, A. Patil, et al., "Synthesis of Green Nanobiofertilizer Using Silver Nanoparticles of *Allium cepa* Extract Short Title: Green Nanofertilizer From *Allium cepa*," *International Journal of Chemical Studies* 8, no. 4 (2020): 1690–1694, https://doi.org/10.22271/chemi.2020.v8.i4q.9854.

18. F. Al-Otibi, S. A. Alfuzan, R. I. Alharbi, et al., "Comparative Study of Antifungal Activity of Two Preparations of Green Silver Nanoparticles From *Portulaca oleracea* Extract," *Saudi Journal of Biological Sciences* 29, no. 4 (2022): 2772–2781, https://doi.org/10.1016/j.sjbs.2021.12.056.